

Forecasting failure locations in 2-dimensional disordered lattices

Estelle Berthier^{a,1}, Mason A. Porter^b, and Karen E. Daniels^a

^aDepartment of Physics, North Carolina State University, Raleigh, NC 27695; and ^bDepartment of Mathematics, University of California, Los Angeles, CA 90095

Edited by Stefano Zapperi, University of Milan, Milan, Italy, and accepted by Editorial Board Member Herbert Levine June 21, 2019 (received for review January 8, 2019)

Forecasting fracture locations in a progressively failing disordered structure is of paramount importance when considering structural materials. We explore this issue for gradual deterioration via beam breakage of 2-dimensional (2D) disordered lattices, which we represent as networks, for various values of mean degree. We study experimental samples with geometric structures that we construct based on observed contact networks in 2D granular media. We calculate geodesic edge betweenness centrality, which helps quantify which edges are on many shortest paths in a network, to forecast the failure locations. We demonstrate for the tested samples that, for a variety of failure behaviors, failures occur predominantly at locations that have larger geodesic edge betweenness values than the mean one in the structure. Because only a small fraction of edges have values above the mean, this is a relevant diagnostic to assess failure locations. Our results demonstrate that one can consider only specific parts of a system as likely failure locations and that, with reasonable success, one can assess possible failure locations of a structure without needing to study its detailed energetic states.

failure | lattices | networks | centrality

Cellular foams (1), semiflexible fiber and polymer networks (2), and many recently developed mechanical metamaterials (3–5) all belong, in idealized form, to a general class of disordered lattices. Such lattices can range in size from microscopic scaffolds for biological tissue growth (6) to modern architectural structures (7). In each case, one can further idealize the material or structure as a mathematical network of connections between slender beams that intersect at various points within the material. From an engineering perspective, such materials are promising because of their light weights and their tunable, designable properties: a Poisson ratio from the auxetic (4, 8, 9) to the incompressible limits (4), a targeted local response to a remote perturbation (5), or the ability to change shape (3). A disadvantage of these materials is that those that are constructed from stiff materials can degrade progressively through successive abrupt failures of the beams during loading (8, 10, 11). To design optimized structures and safely use them for structural applications, it is necessary to assess the most likely locations of fracture. Such predictive understanding would further enable the design of a material to fail in a prescribed way.

Fracture experiments have been conducted previously on printed, disordered auxetic materials (8) and 2-dimensional (2D) laser-cut, disordered honeycomb lattices (10). In these studies, very different fracture behaviors (ductile vs. brittle) have been obtained by changing the loading direction (8) or tuning the rigidity (10). In the latter study, a clear change arose in the spatial organization of fractures: they can either be dispersed throughout a system or be localized in the form of a narrow crack. Therefore, although some tunable parameters for controlling failure behavior have been identified, what determines these particular failure locations remains an open question. According to the theory of Griffith (12), damage in brittle materials focuses at the tip of a crack. However, factors

such as material disorder (13–17), material rigidity (10), and the connectivity (specifically, mean degree) of networks (10, 18) can affect the spatial organization of damage. As one tunes each of these factors, one can make failures spread throughout a system (diffuse damage) rather than form a narrow crack (localized damage).

Zhang and Mao (11) showed recently that failures can also be delocalized in topological Maxwell lattices (in which freely rotating joints that are linked by rigid struts are on the verge of mechanical instability) (19). They performed numerical experiments on the tensile fracture of deformed square and kagome lattices, demonstrating that stress and fracture concentrate on self-stress domain walls, even in the presence of damage that is introduced elsewhere in the system. In another recent paper, Tordesillas et al. (20) studied damage locations in discrete element simulations of concrete samples under uniaxial tension. From a network-flow analysis of the contact-network topology and contact capacities of a specimen, the authors determined the location of the principal interacting macrocracks. In their samples, they observed that secondary macrocracks develop in the prefailure regime after damage occurs elsewhere, but before the formation of a dominant macrocrack that sets the ultimate failure pattern of a sample.

In this paper, we investigate where damage occurs in disordered lattices that consist of identical-width beams, with a network topology specified by contacts that are measured from a real quasi-2D granular packing (Fig. 1). We identify a common property, a large value of geodesic edge betweenness centrality (GEBC) (25), that is shared by the failure locations of progressive damage events of our tested samples. Even without modeling

Significance

Disordered lattices are used widely for mechanical applications because they are lightweight and robust. Due to their heterogeneous structure, it is a complicated task to understand and forecast their progressive degradation. To safely use these materials and design structures with optimized mechanical properties, it is crucial to understand where failures occur. We show that a simple test that consists of comparing the importance of a beam with respect to the other beams in a lattice permits a successful forecast of the locations of failures. It allows one to consider only a small fraction of the beams as likely failure locations. Our approach also provides a roadmap for studies of failures in other spatial networks.

Author contributions: E.B., M.A.P., and K.E.D. designed research, performed research, analyzed data, and wrote the paper, with E.B. as the lead researcher.

The authors declare no conflict of interest.

This article is a PNAS Direct Submission. S.Z. is a guest editor invited by the Editorial Board.

Published under the PNAS license.

¹To whom correspondence may be addressed. Email: ehberthi@ncsu.edu.

This article contains supporting information online at www.pnas.org/lookup/suppl/doi:10.1073/pnas.1900272116/-DCSupplemental.

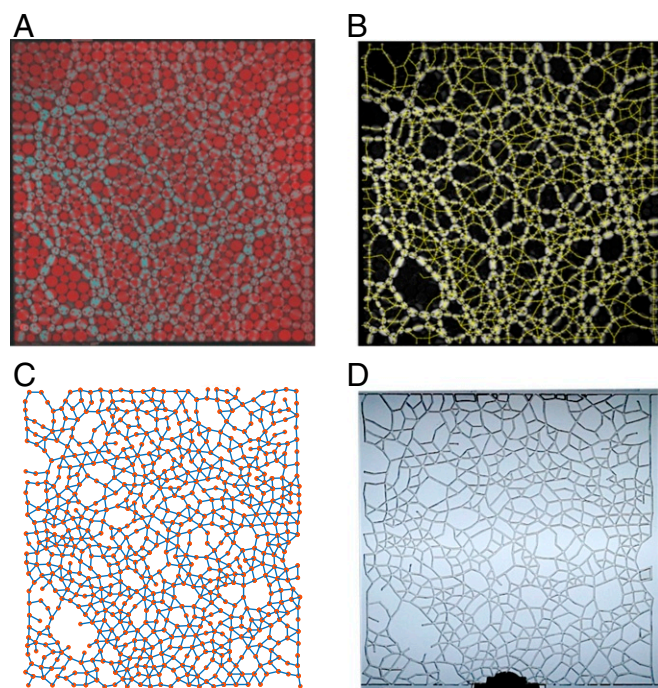


Fig. 1. (A) Force chains (cyan) recorded in a 2D assembly of frictional photoelastic disks (red), which we image via a circular polariscope (21). Brighter particles carry stronger forces. (B) Contact network (yellow), which was extracted using an open-source photoelastic solver (21–23), overlaid on the reconstructed “pseudo-image” (21). (C) Network representation in which each particle center is a node (orange dots) and each load-bearing contact is an edge (blue lines) (24). (D) Corresponding physical sample that we laser cut from an acrylic sheet, with the edges represented by beams that intersect at cross-links (which correspond to the nodes in the network).

the physical interactions between nodes, this property provides a diagnostic for identifying likely failure locations. Such an indicator would permit assessing these locations in a structure without studying its detailed energetic or stress states. Ultimately, the choice of a granular-inspired geometry for a disordered lattice will provide a route toward generalizing these studies across inherently different systems, which are linked by their network topology.

For each network, we laser cut an acrylic sheet using a contact network that matches the one observed in a packing, and we then test its behavior under compressive or tensile loading. Because the set of contacts in a packing forms a network that is embedded in a plane, our lattice does as well. Such a lattice network consists of edges (representing the beams of the lattice) that intersect at nodes, which occur at the cross-links of the lattice. Conceptually similar structures occur in streets and intersections in the study of road networks (26, 27), connections between internet routers, plant veins (28), fungi (29), and many other spatial systems (30, 31).

Network analysis provides useful approaches—including measures, algorithms, and theory—for characterizing complex spatial systems at multiple scales, ranging from local features to mesoscale and macroscale ones, and examining how they evolve (24, 32). As discussed by Smart and Ottino (33), it is appealing to investigate what insights network analysis and associated topics (e.g., graph theory and algebraic topology) can yield on physical systems, especially in comparison with traditional approaches. For example, this perspective was adopted by Tordesillas et al. (20) to study quasibrittle failure using network-flow analysis. Such approaches have also been useful for the study of mesoscale structures, such as dense communities of nodes, in granular sys-

tems (34). Therefore, network analysis seems to be a promising route to identify common analytical tools that are capable of relating failure behaviors across a variety of disordered systems.

One important approach in network analysis is the calculation of “centrality” measures to ascertain the most important nodes, edges, and other subgraphs in a network (32, 35). One particularly popular type of centrality, known as betweenness centrality, measures whether one or more parts of a network lie on many short paths; it has been used to characterize the importance of nodes (36), edges (25), and other subgraphs. The most common type of betweenness centrality uses geodesic (i.e., strictly shortest) paths.

Recently, in a study of granular materials, Kollmer and Daniels (37) showed that there is a positive correlation between the geodesic betweenness centrality value of a node and the pressure on the corresponding particle. Previously, Smart et al. (38) reported that edges with large geodesic betweenness centrality exert a strong influence on heat transport in granular media. Inspired by these investigations, we selected from among the variety of network measures (31, 32) and focus on calculating GEBC. We show its definition in Eq. 5 (see *Materials and Methods*).

As was reported in Berthier et al. (23), one can control the compressive and tensile failure behaviors of a disordered lattice by tuning the mean degree of its associated network. This control parameter provides a way to create systems with a variety of failure behaviors, ranging from ductile-like to brittle-like failure. In this paper, we show for samples across the spectrum from brittle-like to ductile-like failure (see *Mechanical Testing Protocol*) that individual beam failures occur predominantly on edges with GEBC values that are above the mean of the network. From this result, we conclude that GEBC is a useful diagnostic for forecasting possible failure locations in our contact networks. We demonstrate the ability of a GEBC-based test, which consists of comparing the GEBC value of an edge with a threshold value, to discriminate between beams that fail and those that remain intact. This finding, together with the work of ref. 38, suggests that betweenness centrality is a useful measure for capturing essential physical properties in disordered systems. Our study also confirms that tools from network analysis give a promising paradigm for the study of fracture.

The effectiveness of GEBC, which depends on network topology rather than on specifying mechanical interactions, is unexpected. This motivates a deeper analysis to determine which behaviors do not depend primarily on the detailed physical properties of a system, but instead depend on its geometry (and associated network topology). Our use of unweighted networks focuses our investigation on network topology, and we compare results for both a measure (specifically, GEBC) that ignores the physics and a well-known scalar electrical analogy of elasticity known as a random fuse network (RFN) model (17, 39). The RFN model identifies the most stressed beams as the edges with the largest currents, as determined by solving Kirchhoff’s laws, for a given voltage drop across the boundaries. We show that the RFN model, even with its incorporation of physical considerations, does not markedly improve performance over GEBC. This indicates that one can capture essential features of lattice failure behavior by geometric (rather than physical) considerations.

Results

Spatial Heterogeneity and Changes with Applied Strain of GEBC.

We examine the ability of GEBC \tilde{E} (Eq. 5) to forecast the specific locations at which our samples fail. For each initial (and subsequently altered) network, we find that geodesic edge betweenness takes a broad range of values across the network. In Fig. 24, we show the probability density function (PDF) of the initial geodesic edge betweenness \tilde{E}_0 for each initial network at each value of the mean degree \bar{z}_0 . To facilitate notation,

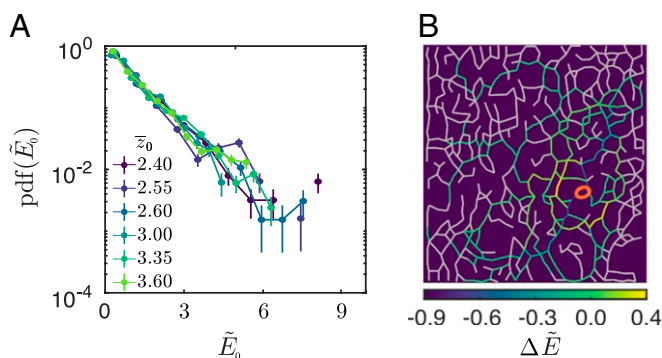


Fig. 2. Characterization of geodesic edge betweenness (re-)distribution. (A) PDF of the initial GEBC \tilde{E}_0 for the different initial networks. We show the PDFs for several values of mean degree. (B) Changes in GEBCs \tilde{E} after a failure event that occurs at the red ellipse at a compressive strain of $\epsilon \approx 1.98\%$ on a network with mean degree $\bar{z}_0 = 2.40$. The values of the lavender edges change by less than 10^{-2} .

we use the subscript 0 to designate our initial networks and the quantities that we measure and compute with them. In all cases, the distribution of values is approximately exponential, and it is largely independent of \bar{z}_0 . Because each failure event (with associated edge removals) results in a new set of shortest paths, we obtain a new distribution of GEBC values for each altered network. Just as stress redistributes after damage (40–43), GEBC (due to its nonlocal nature) also redistributes in a system. In Fig. 2B, we show a characteristic example of redistribution after a failure event. The redistributions are system-wide: some edges are “reloaded,” becoming more important with respect to the others (i.e., $\tilde{E}_{s+1} > \tilde{E}_s$ when going from strain step s to strain step $s+1$), others are “unloaded” (i.e., $\tilde{E}_{s+1} < \tilde{E}_s$), and some edges (in lavender in Fig. 2B) have the same (or almost the same) value. By contrast, removal of unimportant edges (i.e., those with small values of GEBC) results in small (in amplitude) changes.

Damage occurs progressively through a sequence of tensile or compressive loading. In Fig. 3, we show examples of damage progression for 3 values (1 per row) of \bar{z}_0 . Within each row, a sample progresses from its initial intact network G_0 (an unweighted and undirected graph) through an altered network at which about 50% of its beams have failed, and then to the network immediately before the final failure. For each row of Fig. 3, in the network immediately after the last image that we show, there is no longer a set of beams that connects the top and bottom boundaries of the sample. We color each edge in each network according to the value of \tilde{E}_s at that strain step.

Geodesic edge betweenness is spatially heterogeneous across a network, and we observe that large values (bright colors) can occur throughout a network. These locations shift both in space and in time due to the disordered structure (which arises from geometry) of our lattices. By contrast, for a regular lattice, the importance of edges decreases with their distance from the geometric center of a system (31). The introduction of disorder—such as by rewiring, addition, or removal of edges—results in more complicated distributions and can lead to geographically central edges with smaller importance than elements that are farther from the geometric center (44). Importantly, although the topologies of the networks underlying our lattices are inherited from uniaxially compressed granular packings, we do not observe a preferred orientation for edges with GEBC values that are above the mean. Granular packings encode their preparation history in the form of anisotropic stresses (45, 46), but this anisotropy is not readily identifiable from the contact network (which is unweighted).

The GEBC values at a given strain step illustrate the broad distribution of values, as we observed in the exponential PDF of \tilde{E}_0 (Fig. 2). Even in these small systems, some edges have values up to 20 times the mean of the system; these are ones that are particularly important for connecting different parts of a network. Many other edges occur only infrequently as shortest-path connectors. The variations in spatial distribution along the rows of Fig. 3 highlight the importance of the removed edges, as we emphasized in Fig. 2B. Importantly, although \tilde{E} tends to decrease with distance from the geometric center, this need not be true for specific samples. For the near-final networks (Fig. 3, Right) at $\bar{z}_0 = 2.40$ and $\bar{z}_0 = 3.00$, the maximum of \tilde{E} is located near the left boundary of the sample, rather than near the middle. In both cases, the largest values of \tilde{E} occur on edges that connect the top and bottom parts of the network, and these are also the next beams that will break (and lead to the final cascade of failures).

GEBCs of Failed Edges. Such observations suggest that there is a correlation between large values of \tilde{E} and future failure locations. To assess the generality of this finding, for each breaking beam, we calculate the GEBC \tilde{E}_f during step $s-1$ immediately before its failure at step s . For all of our samples and for all small failure events (which we take to mean that no more than 3 beams are involved), we enumerate the immediately preceding values of \tilde{E} for the failed edges. In Fig. 4A, we show the cumulative distribution function (CDF) of this set of values, together with the corresponding PDF in Fig. 4A, Inset. We fit the PDF with an exponential with mean $\tilde{E}_f^* \approx 10.3$ (with $R^2 \approx 0.96$). There is a corresponding gradual increase for $\tilde{E}_f \gtrsim 10$ of the CDF, suggesting that few failing edges have a value that is significantly larger than the mean. We observe such large values of \tilde{E} only when the samples are near full failure; at this point, only a few paths are available to connect the top and bottom boundaries of the network. One can see this situation in Fig. 3, Right. Focusing on $\tilde{E}_f = 1$, we see that about 76% of the breakages occur on edges with values of \tilde{E}_f that are above the mean. Because only a small subset of the network's edges have $\tilde{E} > 1$ (see the distribution in Fig. 2A), even the value of \tilde{E} alone is a valuable diagnostic for forecasting failure locations.

We can refine this diagnostic by directly considering the population of edges that exceed a threshold value \tilde{E}_{th} . We illustrate this population by plotting the complementary cumulative distribution function (CCDF) on the left vertical axis in Fig. 4B. Because the proportion of edges that satisfy $\tilde{E} > \tilde{E}_{th}$ evolves after each edge removal and differs across initial networks, we choose each point of the curve to be the maximum value that we encounter among all networks. The success rate of this diagnostic is the fraction of failed beams that satisfy $\tilde{E} > \tilde{E}_{th}$, and the failure rate is the fraction for which $\tilde{E} \leq \tilde{E}_{th}$. We show the latter as orange diamonds on the right vertical axis of Fig. 4B for all small failure events among all tested samples, regardless of the tensile or compressive nature of the applied loading. In Fig. 4C, we focus on the point at which the CCDF and the failure-rate curves cross; this intersection occurs at $\tilde{E}_{th} \approx 1.1$, corresponding to a value on the CCDF curve (i.e., the fraction of edges for which $\tilde{E} \gtrsim 1.1$) of about 0.34 and a failure rate of about 0.26. This intersection point indicates that considering all edges with above-mean GEBC values provides a reasonable population of edges to consider, but one can choose other values in a tradeoff between forecast failure rate and the fraction of examined edges.

The above general results exhibit sample-to-sample variation. To highlight this, we include an envelope of the failure rate in

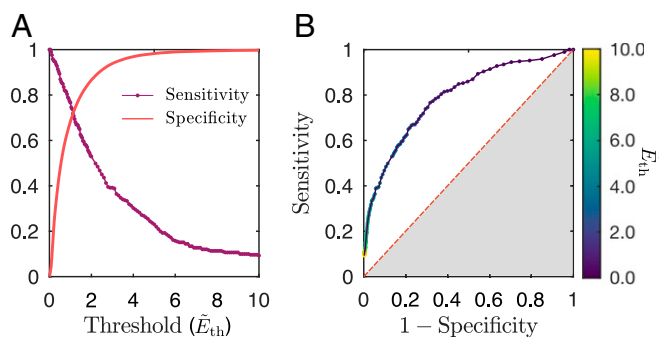


Fig. 5. Evaluation of our test's accuracy. (A) Sensitivity and specificity vs. the threshold \tilde{E}_{th} . (B) ROC curve summarizing the (sensitivity, $1 - \text{specificity}$) pairs that we obtain for different values of \tilde{E}_c . The dashed diagonal line indicates the behavior of a test that cannot discriminate between failing and intact beams.

such correlations also depends on network type) (27). Therefore, different measures related to betweenness can give complementary insights.

Comparison with Other Diagnostics. To disentangle the roles of physical and geometric effects, we evaluate the importance of introducing physical considerations by repeating our analysis using an RFN-based test (see *RFN Model*). In place of \tilde{E} , we determine the current \tilde{I} that flows through a network. As with GEBC, we determine the fraction of edges in a network with a current above a threshold current \tilde{I}_{th} and the fraction of failing beams for which $\tilde{I}_f \leq \tilde{I}_{th}$ (where \tilde{I}_f denotes the current of an edge during step $s - 1$ immediately before its failure at step s).

For threshold values in the range $[0, 2.5]$, we find that this test performs somewhat better than the test using GEBC (*SI Appendix, Fig. S1A*). However, in the range $[0, 1.4]$, the fraction of edges with a current above the threshold is slightly larger than the fraction of edges with a GEBC above the same threshold. Consequently, the tradeoff between the forecast failure rate and the fraction of possible edges differs between the 2 tests for the same threshold value. This tradeoff diminishes the advantage.

We also find that the current and GEBC values of the failed edges are positively correlated, with a Pearson correlation coefficient of $R \approx 0.81$ (*SI Appendix, Fig. S1B*). This suggests that failing beams, most of which have a larger stress than the mean value in a network (i.e., $\tilde{I}_f > 1$ for these edges), lie on many shortest paths, explaining the small improvement in forecast capability from using the RFN-based test. This finding is similar to the results of Kollmer and Daniels (37), who observed in 2D packings of frictional particles that ones with large node betweenness centralities are statistically likely to be highly stressed. Consequently, it is appropriate to examine betweenness centralities (of both nodes and edges) to capture important mechanical properties of physical systems.

Interestingly, as we show in *SI Appendix, Fig. S2*, the 2 tests do not systematically misdiagnose failure locations (i.e., yield FN outputs) for the same edges. Using the RFN-based test, we observe a correlation between beam angle and current flow (*SI Appendix, Fig. S3A*) and find a bias toward misdiagnosed edges that are roughly perpendicular to the loading direction (*SI Appendix, Fig. S3B*). It seems that failures occur at edges at all distances from the boundaries (*SI Appendix, Fig. S4A*). However, for some threshold values, most GEBC-misdiagnosed edges tend to occur near boundaries (*SI Appendix, Fig. S4B*), where large values of GEBC are less frequent.

The dependency of GEBC with distance from a sample's geometric center, even altered by the presence of disorder, is an important feature of networks that are embedded in a plane. To

examine whether we can circumvent this limitation of our GEBC test, we calculate GEBCs on a collection of modified networks. For a given network G and for each edge e_{ij} , we generate a duplicated network such that the edge e_{ij} is at the geometric center. To construct such a graph, we first duplicate the network with mirror symmetries with respect to each boundary. We then calculate the GEBC of e_{ij} by considering only a section of this duplicated network that is approximately centered at e_{ij} . We repeat this procedure for each edge of the network G to obtain centrality values for the network centered at that edge. Using this approach yields a cumulative distribution for \tilde{E}_f and a test ($\tilde{E}_f > \tilde{E}_{th}$) success rate similar to the original networks. Indeed, although boundary edges can have large \tilde{E} values, the distributions of \tilde{E} are more homogeneous than in the original networks, such that the test can misdiagnose edges in other locations. Consequently, the use of a duplicated network does not improve the forecasting ability of our approach. Preliminary calculations that account for the boundaries' loading (using master particles that are adjacent to corresponding loaded nodes) suggest that this simple physical consideration provides a way to improve our test's ability to forecast failure locations. Developing methods to appropriately consider the role of boundaries remains a central question for planar graphs—not only for granular materials, but also for other applications, such as determining high-traffic edges in road networks (27) and nutrient transportation networks (29)—and more generally in spatially-embedded networks.

In our comparison of GEBC-based and RFN-based tests, we observe a correlation between the physical and geometric properties of failing beams. Interestingly, a test that includes a minimal set of physical ingredients (i.e., the RFN-based test) performs only somewhat better than a test (the GEBC-based test) that is based on geometric considerations. Because these 2 tests have rather different limitations—with less successful forecasting of near-perpendicular edges vs. near-boundary edges—it is useful to use both as complementary approaches. Finally, it is worth noting that, although the RFN-based test is faster computationally than the GEBC-based one, neither approach requires significant computational resources for the system sizes that we consider in this study.

Conclusions

The idea, proposed in papers such as ref. 33 and reviewed in ref. 24 in the context of granular and particulate systems, to use network analysis to achieve insights on physical systems seems very promising for studies of fracture. In this paper, we explored the application of centrality measures (based on shortest paths) to forecast failure locations in physical samples. Many other tools from network analysis, such as those based on exploration of mesoscale structures, also promise to yield fascinating insights into investigations of physical networks. In particular, examining how network analysis can contribute to forecasting not only where, but also when, failures occur in disordered networks is a central point for future studies.

In our investigation, we found that calculations based on shortest paths can help forecast failure locations in disordered lattices. Specifically, calculating the geodesic betweennesses of the edges in a network permits one to assess which edges are more prone to failure than others. Considering only edges with values above the mean GEBC of a network allows one to discard a large fraction of edges as unlikely failure locations. This feature of our test makes it very valuable, especially because it avoids a detailed analysis of energetics.

Combined with refs. 37 and 38, our work provides evidence that betweenness centrality successfully identifies physical properties in both granular packings and lattices that are derived from them. Similarly, analyses inspired by rigidity percolation

edges is $\mathcal{O}(Nm)$ for sparse networks, where N and m denote the numbers of nodes and edges, respectively, of a network (25). All of our graphs G are undirected and unweighted, but one can also study notions of edge betweenness centrality for directed and weighted graphs.

It is common to normalize E_{ij} by $\frac{1}{2}N(N-1) - 1$ (i.e., the number of edges other than the one under consideration) (57) or by $(N-1)(N-2)/2$ (i.e., the number of node pairs) (31) to ensure that GEBC values lie between 0 and 1. However, because we compare the relative importance of edges to others in a given network and as successive edge removals occur, we use a different normalization. In our calculations, for a given network at strain step s and characterized by its adjacency matrix A_s (where $s = 0$ for the initial network), we define the normalized GEBC matrix $\bar{E}_s = E_s/\bar{E}_s$, where \bar{E}_s is the mean over all edges of the network G_s . To study the importance of the failing beams, for each strain step, we compute the matrix \bar{E}_s and extract the values \bar{E}_f of the edges that fail in the next failure event.

RFN Model. We create an RFN (17, 39) in which each fuse matches an edge of the network for one of our samples. All fuses have identical conductance,

because the beams have identical thickness. We load the top and bottom boundaries by applying a fixed voltage to the top nodes and connecting the bottom nodes to ground (0 voltage). We determine edge voltages and their associated currents by solving Kirchhoff's laws. Analogous to our examination of GEBC, we normalize the current by the mean over all edge currents in a network. We define a current matrix at strain step s by $\bar{I}_s = I_s/\bar{I}_s$, where $s = 0$ denotes the initial network and associated quantities. We then proceed as with GEBC: for each strain step s , we calculate the matrix \bar{I}_s and extract the normalized current (i.e., stress) \bar{I}_f of the edges that fail in the next failure event.

ACKNOWLEDGMENTS. We acknowledge Jonathan Kollmer for sharing the granular force-network data that were collected for ref. 23. We also thank Danielle Bassett for her fruitful advice on boundary considerations. We thank 2 anonymous referees for their many helpful comments, and we are also particularly thankful to referee 2 for the suggestion to use the RFN-based test to perform a deeper analysis. This research was supported by the James S. McDonnell Foundation.

1. L. J. Gibson, M. F. Ashby, G. S. Schajer, C. I. Robertson, The mechanics of two-dimensional cellular materials. *Proc. R. Soc. A* **382**, 25–42 (1982).
2. C. Broedersz, F. MacKintosh, Modeling semiflexible polymer networks. *Rev. Mod. Phys.* **86**, 995–1036 (2014).
3. K. Bertoldi, V. Vitelli, J. Christensen, M. van Hecke, Flexible mechanical metamaterials. *Nat. Rev. Mater.* **2**, 17066 (2017).
4. C. P. Goodrich, A. J. Liu, S. R. Nagel, The principle of independent bond-level response: Tuning by pruning to exploit disorder for global behavior. *Phys. Rev. Lett.* **114**, 225501 (2015).
5. J. W. Rocks *et al.*, Designing allostery-inspired response in mechanical networks. *Proc. Natl. Acad. Sci. U.S.A.* **114**, 2520–2525 (2017).
6. P. A. Janmey, J. P. Winer, J. W. Weisel, Fibrin gels and their clinical and bioengineering applications. *J. R. Soc. Interf.* **6**, 1–10 (2009).
7. J. Knippers, K. G. Nickel, T. Speck, *Biomimetic Research for Architecture and Building Construction, Biologically-Inspired Systems* (Springer International Publishing, Cham, Switzerland, 2016).
8. M. Hanifpour, C. F. Petersen, M. J. Alava, S. Zapperi, Mechanics of disordered auxetic metamaterials. *Eur. Phys. J. B* **91**, 271 (2018).
9. D. R. Reid *et al.*, Auxetic metamaterials from disordered networks. *Proc. Natl. Acad. Sci. U.S.A.* **115**, E1384–E1390 (2018).
10. M. M. Driscoll *et al.*, The role of rigidity in controlling material failure. *Proc. Natl. Acad. Sci. U.S.A.* **113**, 10813–10817 (2016).
11. L. Zhang, X. Mao, Fracturing of topological Maxwell lattices. *New J. Phys.* **20**, 063034 (2018).
12. A. A. Griffith, VI. The phenomena of rupture and flow in solids. *Phil. Trans. R. Soc. Lond. A* **221**, 163–198 (1921).
13. S. Roux, A. Hansen, H. Herrmann, E. Guyon, Rupture of heterogeneous media in the limit of infinite disorder. *J. Stat. Phys.* **52**, 237–244 (1988).
14. M. J. Alava, P. K. V. V. Nukala, S. Zapperi, Role of disorder in the size scaling of material strength. *Phys. Rev. Lett.* **100**, 055502 (2008).
15. A. Shekhawat, S. Zapperi, J. P. Sethna, From damage percolation to crack nucleation through finite size criticality. *Phys. Rev. Lett.* **110**, 185505 (2013).
16. W. A. Curtin, H. Scher, Brittle fracture in disordered materials: A spring network model. *J. Mater. Res.* **5**, 535–553 (1990).
17. B. Kahng, G. G. Batrouni, S. Redner, L. de Arcangelis, H. J. Herrmann, Electrical breakdown in a fuse network with random, continuously distributed breaking strengths. *Phys. Rev. B* **37**, 7625–7637 (1988).
18. L. Zhang, D. Z. Rocklin, L. M. Sander, X. Mao, Fiber networks below the iso-static point: Fracture without stress concentration. *Phys. Rev. Mater.* **1**, 052602(R) (2017).
19. X. Mao, T. C. Lubensky, Maxwell lattices and topological mechanics. *Ann. Rev. Condens. Matter Phys.* **9**, 413–433 (2018).
20. A. Tordesillas, S. Kahagallage, C. Ras, M. Nitka, J. Teichman, Interdependent evolution of robustness, force transmission and damage in a heterogeneous quasi-brittle granular material: From suppressed to cascading failure. arXiv:1809.01491 (30 August 2018).
21. K. E. Daniels, J. E. Kollmer, J. G. Puckett, Photoelastic force measurements in granular materials. *Rev. Sci. Instrum.* **88**, 051808 (2017).
22. Berthier *et al.*, Data from “Rigidity percolation control of the brittle-ductile transition in disordered networks.” Dryad Digital Repository. <https://doi.org/10.5061/dryad.q1g5279>. Accessed 17 July 2019.
23. E. Berthier *et al.*, Rigidity percolation control of the brittle-ductile transition in disordered networks. *Phys. Rev. Mater.* **3**, 075602 (2019).
24. L. Papadopoulos, M. A. Porter, K. E. Daniels, D. S. Bassett, Network analysis of particles and grains. *J. Complex Networks* **6**, 485–565 (2018).
25. M. Girvan, M. E. J. Newman, Community structure in social and biological networks. *Proc. Natl. Acad. Sci. U.S.A.* **99**, 7821–7826 (2002).
26. P. Crucitti, V. Latora, S. Porta, Centrality measures in spatial networks of urban streets. *Phys. Rev. E* **73**, 036125 (2006).
27. S. H. Lee, M. Cucuringu, M. A. Porter, Density-based and transport-based core-periphery structures in networks. *Phys. Rev. E* **89**, 032810 (2014).
28. E. Katifori, M. O. Magnasco, Quantifying loop network architectures. *PLoS One* **7**, e37994 (2012).
29. S. H. Lee, M. D. Fricker, M. A. Porter, Mesoscale analyses of fungal networks as an approach for quantifying phenotypic traits. *J. Complex Networks* **5**, 145–159 (2017).
30. M. Barthelemy, Spatial networks. *Phys. Rep.* **499**, 1–101 (2011).
31. M. Barthelemy, *Morphogenesis of Spatial Networks* (Lecture Notes in Morphogenesis, Springer International Publishing, Cham, Switzerland, 2018).
32. M. E. J. Newman, *Networks* (Oxford Univ Press, Oxford, UK, ed. 2, 2018).
33. A. Smart, J. M. Ottino, Granular matter and networks: Three related examples. *Soft Matter* **4**, 2125–2131 (2008).
34. D. S. Bassett, E. T. Owens, K. E. Daniels, M. A. Porter, Influence of network topology on sound propagation in granular materials. *Phys. Rev. E* **86**, 041306 (2012).
35. S. Wasserman, K. Faust, *Social Network Analysis: Methods and Applications* (Cambridge Univ Press, Cambridge, UK, 1994).
36. L. C. Freeman, A set of measures of centrality based on betweenness. *Sociometry* **40**, 35–41 (1977).
37. J. E. Kollmer, K. E. Daniels, Betweenness centrality as predictor for forces in granular packings. *Soft Matter* **15**, 1793–1798 (2019).
38. A. Smart, P. Umbanhowar, J. Ottino, Effects of self-organization on transport in granular matter: A network-based approach. *Europhys. Lett.* **79**, 24002 (2007).
39. L. de Arcangelis, S. Redner, H. Herrmann, A random fuse model for breaking processes. *J. Phys. Lett.* **46**, 585–590 (1985).
40. M. J. Alava, P. K. V. V. Nukala, S. Zapperi, Statistical models of fracture. *Adv. Phys.* **55**, 349–476 (2006).
41. S. Zapperi, A. Vespignani, H. E. Stanley, Plasticity and avalanche behaviour in microfracturing phenomena. *Nature* **388**, 658–660 (1997).
42. R. C. Hidalgo, Y. Moreno, F. Kun, H. J. Herrmann, Fracture model with variable range of interaction. *Phys. Rev. E* **65**, 046148 (2002).
43. E. Berthier, V. Démery, L. Ponson, Damage spreading in quasi-brittle disordered solids. I. Localization and failure. *J. Mech. Phys. Sol.* **102**, 101–124 (2017).
44. B. Lion, M. Barthelemy, Central loops in random planar graphs. *Phys. Rev. E* **95**, 042310 (2017).
45. T. S. Majumdar, R. P. Behringer, Contact force measurements and stress-induced anisotropy in granular materials. *Nature* **435**, 1079–1082 (2005).
46. E. S. Bililign, J. E. Kollmer, K. E. Daniels, Protocol dependence and state variables in the force-moment ensemble. *Phys. Rev. Lett.* **122**, 038001 (2019).
47. A. M. Šimundić, Measures of diagnostic accuracy: Basic definitions. *Electron. J. Int. Fed. Clin. Chem. Lab Med.* **19**, 203–211 (2009).
48. M. H. Zweig, G. Campbell, Receiver-operating characteristic (ROC) plots: A fundamental evaluation tool in clinical medicine. *Clin. Chem.* **39**, 561–577 (1993).
49. M. Barthelemy, Betweenness centrality in large complex networks. *Eur. Phys. J. B* **38**, 163–168 (2004).
50. S. Scellato, A. Cardillo, V. Latora, S. Porta, The backbone of a city. *Eur. Phys. J. B* **50**, 221–225 (2006).
51. Brain connectivity toolbox. <https://sites.google.com/site/bctnet/>. Accessed 30 August 2018.
52. W. G. Ellenbroek, Z. Zeravcic, W. van Saarloos, M. van Hecke, Non-affine response: Jammed packings vs. spring networks. *Europhys. Lett.* **87**, 34004 (2009).
53. W. G. Ellenbroek, V. F. Hagh, A. Kumar, M. F. Thorpe, M. van Hecke, Rigidity loss in disordered systems: Three scenarios. *Phys. Rev. Lett.* **114**, 135501 (2015).
54. M. Wyart, On the rigidity of amorphous solids. *Ann. Phys. Fr.* **30**, 1–96 (2005).
55. S. Henkes, D. A. Quint, Y. Fily, J. Schwarz, Rigid cluster decomposition reveals criticality in frictional jamming. *Phys. Rev. Lett.* **116**, 028301 (2016).
56. U. Brandes, A faster algorithm for betweenness centrality. *J. Math. Sociol.* **25**, 163–177 (2001).
57. G. Chen, X. Wang, X. Li, “Preliminaries” in *Fundamentals of Complex Networks* (Wiley-Blackwell, Hoboken, NJ, 2015), pp. 15–101.